Patterned Assembly of Inorganic Semiconducting Nanowires using Lithography-free Technique

Luca De Pamphilis, Abhishek Singh Dahiya, Adamos Christou, Sihang Ma, and Ravinder Dahiya

***Abstract*—Patterned assembly of inorganic nanowires (NWs) at desired locations offers the opportunity to realise large-area high performance flexible electronics. Transfer and Contact printing methods are some of the viable methods to achieve this. However, some of the fabrication steps in these methods rely on lithography, which are inherently wasteful and therefore, the approach is not an ideal solution for large area electronics. Herein, we show a lithography-free patterning technique in which NWs are selectively removed from a uniformly contact printed electronic layer. The NWs are removed using an elastomeric stamp. The removal efficiency is improved by evaporating a thin layer of water onto its patterned face, which greatly enhances the stamp-NW adhesion via the capillary action. The SEM analyses of the NW layer showed a good pattern fidelity, fair retention of the initial NW density and optimal contrast between positive and negative areas of the pattern. The efficacy of the presented technique for printed electronics is demonstrated by fabricating all-printed ZnO NW-based photodetectors (PDs) on a flexible substrate. Using the as-prepared patterned NWs, a 3×4 array of PD devices is fabricated. The PDs show good responsivity (1.3×10^6 A/W) and specific detectivity (6.95×10^{16} Jones) in the UV range. These devices show that the presented selective removal approach could be an attractive route for future lithography-free printed electronics.**

***Index Terms*—Flexible electronics, Lithography free Patterning, ZnO nanowires, Photodetectors, Printed Electronics**

I. INTRODUCTION

One-dimensional inorganic semiconducting nanomaterials have been extensively explored for high-performance flexible devices including transistors [1, 2], sensors [3-5], energy harvesters [6-8] etc. This is because of their exciting physical, optical, and electronic properties including high excitonic binding energy, excellent charge transport, high aspect ratio etc. [9-11]. Accordingly, considerable efforts have been made to develop effective means for integration of nanowires (NWs) on flexible/plastic substrates [12-17]. For example, methods such as Langmuir–Blodgett (LB) [18], spray-coating [19], float assembly [20] etc. have been used in conjunction with lithography steps to integrate NWs at selective locations (patterning) and various devices from them [9-13, 21-23].

Among various NW assembly/integration approaches, contact printing offers unique advantages such as: (i) highly directional alignment of NWs in a single-step process, (ii) cost-effectiveness, (iii) negligible contamination, as it is a dry printing method, (iv) possibility to print different types of NWs including heterostructures with unique electronic/optical properties, and (v) possibility for selective printing of NWs. Briefly, the process involves bringing a donor substrate having vertically grown NWs in contact with a receiver substrate and a sliding them at an optimum speed and pressure [24]. The shear forces generated during the sliding process result in breaking the NWs from the fixed end and in their transfer onto the receiver substrate. The NWs are then preferentially aligned along the sliding direction. The obtained NWs based electronic layer is then patterned using photolithography and surface functionalisation [23, 25-27]. Whilst this approach takes advantage of mature micro/nanofabrication technology, the photolithography-enabled patterning is a wasteful process [28]. A lithography-free process for selective printing of NWs can address these issues and can open new opportunities for eco-friendly and sustainable manufacturing of future electronics.

Herein, we present a novel lithography-free and scalable approach– called *selective removal*– to pattern NW layers and show its effectiveness by fabricating an array of high performance ultraviolet (UV) photodetectors (PD). The presented method for selective removal of uniformly printed NWs can be suitable for large area and contamination-free assembly of NWs. The developed selective removal process is schematically illustrated in Fig. 1a-i. The process consists of a patterned polydimethylsiloxane (PDMS) stamp to pick printed NWs from the pre-selected locations. To enhance the yield of NW removal, just before the PDMS stamp and NW layer are contacted, the former was exposed to water vapours to improve its adhesive capability. After contact, the PDMS stamp was lifted from the substrate having the NW-based electronic layer. The removal efficacy and fidelity studies are performed on the NW layer contact printed on Si/SiO_2 substrates. The results show that the method can pattern NW layers with a good retention of the pristine NW density and an optimal density contrast between the areas in the pattern and the ones outside. It is noteworthy to mention that the approach allows patterning of a wide range of nanomaterials assembled using other techniques such as LB, spray-coating etc.

The presented work extends our initial study reported in [29].

This work was supported in part by the European Commission, through the NeuTouch Innovative Training Network (H2020-MSCA-ITN-2018-813713), and by the Engineering and Physics Sciences Research Council through Engineering Fellowship for Growth (EP/R029644/1) and Hetero-Print Programme Grant (EP/R03480X/1). An earlier version of this paper was presented at 2022 IEEE International Conference on Flexible and Printable Sensors and Systems (FLEPS) (DOI: 10.1109/FLEPS53764.2022.9781514). (Corresponding author: Ravinder Dahiya)

L. De Pamphilis, A. S. Dahiya, S. Ma, and A. Christou are with the Bendable Electronics and Sensing Technologies (BEST) Group, James Watt School of Engineering, University of Glasgow, Glasgow G12 8QQ, U.K.

R. Dahiya is with Bendable Electronics and Sustainable Technologies (BEST) Group, ECE Department, Northeastern University, Boston, MA 02115, USA. This work in this paper was initiated by R. Dahiya's Bendable Electronics and Sensing Technologies (BEST) Group when he was at University of Glasgow, UK. The work was completed after he moved to Northeastern University, where his group is known as Bendable Electronics and Sustainable Technologies (BEST) Group (email – r.dahiya@northeastern.edu)

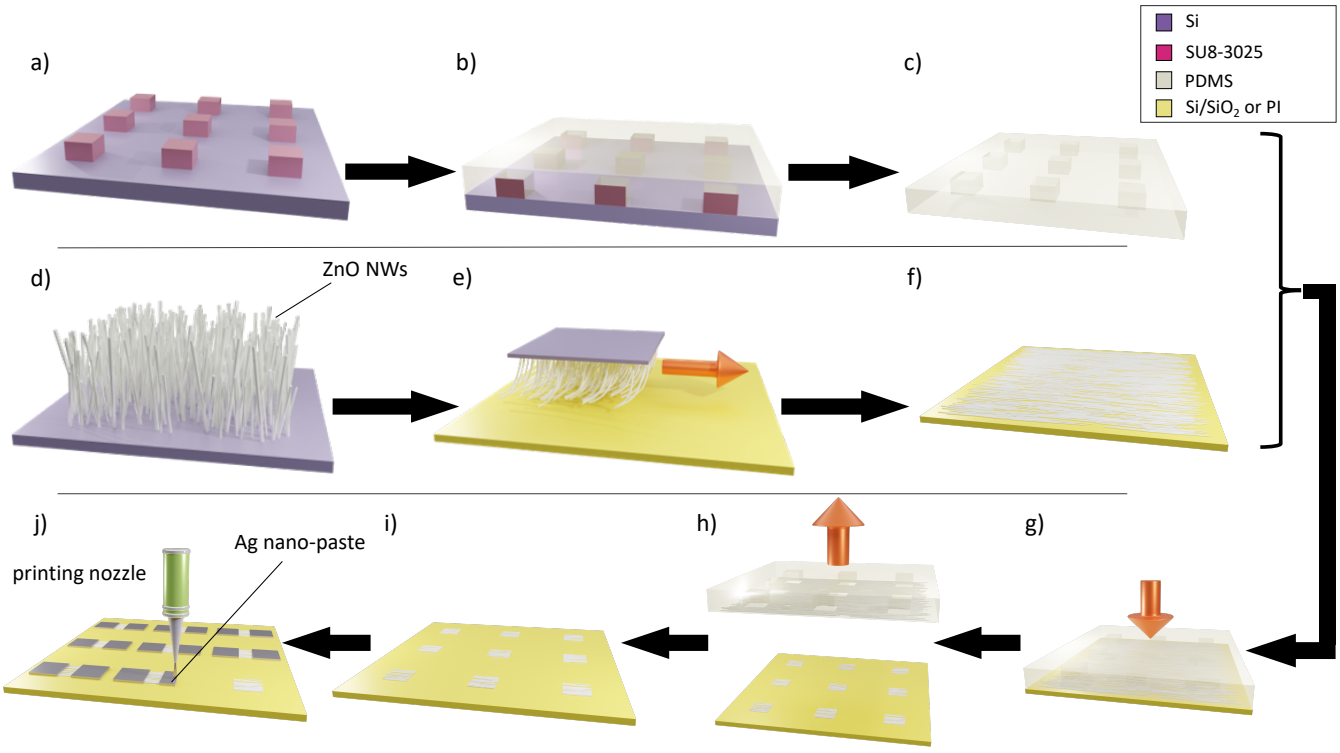

Fig. 1. Schematic illustration of the patterned NW-based device fabrication. First, micropatterned elastomer stamp is fabricated, through a) master mould, b) PDMS layer curing on top of the mould, c) release of patterned PDMS stamp. In parallel, contact printing of ZnO NWs layer is obtained: d) ZnO NW growth on the donor substrate, e) contact printing on the receiver substrate and (f) obtained NW layer. In the end, NWs are selectively removed, and PDs are fabricated: g) water vapours-exposed stamp contacting the NWs layer, h) stamp release with the (i) obtained patterned NW layer and (j) electrodes printing via extruded silver paste.

The initial work presented in IEEE FLEPS conference used an arbitrary stamp to remove NWs in small squares of the contact printed layer. Here, we have used a new PDMS stamp which is carefully designed to remove NWs from everywhere except from 100 × 100 μm^2 squares. The micropatterned stamp was obtained by curing PDMS on a master mould, which consists of a pattern of cured negative photoresist pillars on a Si substrate. Further, to demonstrate the viability of our approach, we used it to print NW patterns on a flexible polyimide (PI) substrate. The as-prepared patterned NW array was used to develop a batch of all-printed PDs. A high-resolution extrusion-based Direct Ink Write (DIW) printer was then employed to define metal electrodes (Fig. 1j). The fabricated 3×4 array of PDs exhibits excellent UV response including responsivity of 1.3×10^6 A/W, specific detectivity of 6.95×10^{16} Jones, and current on/off ratio of 1.19×10^4.

This paper is organised as follows: Section II describes the experimental procedure for NW synthesis, contact printing, PDMS stamp fabrication and selective removal of NWs, and the fabrication of PDs on PI substrate. The studies performed to realise the patterned NW array, to evaluate the effectiveness of contact removal and the PD opto-electrical characterisations are presented in Section III. Finally, Section IV summarises the key findings of this work and proposes the broader field of applications of the demonstrated method.

II. Experimental Section

A. ZnO NW synthesis

ZnO NWs were synthesised via Vapour Phase Transport (VPT) technique. The ZnO powder was mixed with carbon powder (1:1 weight ratio) to generate Zn source vapours through carbothermal reduction of the ZnO powder on top of an Au nanoparticle (NP)-decorated Si (100) substrate. The details of the growth process are reported elsewhere [30-32]. In brief, Au NPs of 80nm diameter were deposited on the Si (100) substrates via drop casting. The Au NP-decorated Si substrates were then placed on top of an alumina boat crucible (Au NPs facing down). The crucible was inserted in a horizontal quartz tube furnace maintained in an argon ambient. The sample was heated to 880°C to allow the carbothermal reduction of ZnO to occur (source materials is mixed ZnO and carbon powder), producing Zn(g) and O_2(g) species that are carried to the Au NP-decorated substrate via Ar as carrier gas. The Au NPs act as catalysts for the Vapour-Liquid-Solid NW growth. The furnace was kept at 880°C for 120 min and then allowed to cool down to room temperature.

B. ZnO NW contact printing

The Si substrates with as-grown ZnO NWs are used as donor substrates. The employed receiver substrates are either rigid Si/SiO_2 or spin coated flexible PI. Prior to the contact printing of NWs, the Si/SiO_2 substrate was sequentially cleaned with acetone, IPA, and DI water. The PI substrate was obtained by

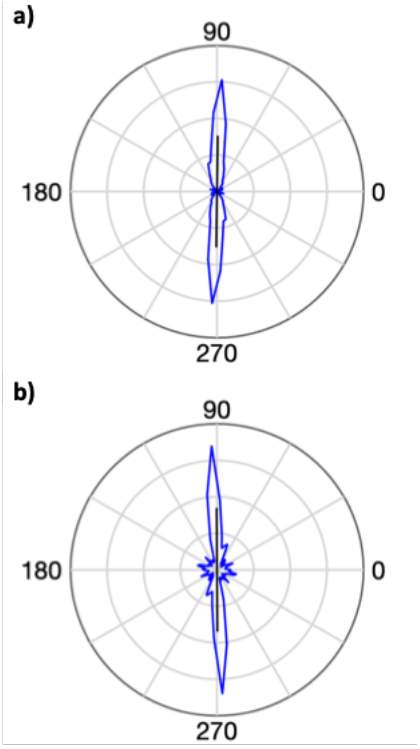

Fig. 2. NW angular distribution in polar coordinates (the black segment represents the average distribution, mainly due to the SEM camera orientation with respect to the sample) of the ZnO NW on Si/SiO_2 contact printed sample a) before and (b) after selective removal, in positive pattern areas. The angles are expressed in arc degrees (°).

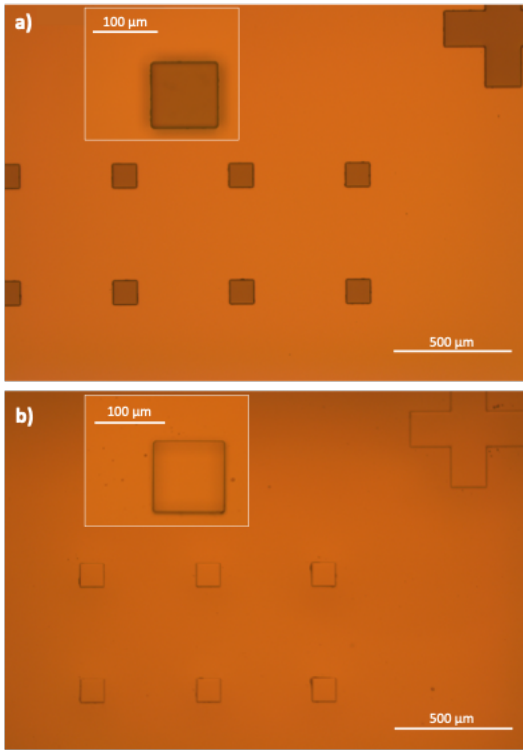

Fig. 3. Optical images of the micropatterned surfaces of (a) the master mould (in the inset, detail of a SU8-3025 pillar), (b) the elastomer stamp (in the inset, detail of the trench).

spin coating two layers of PI on a glass carrier substrate. Briefly, the glass slide was first cleaned with acetone, IPA, and DI water. Then, an Ar plasma treatment (100W for 60s) was performed. Each layer of PI was obtained by spin coating PI 2525 (by HQ MicroSystems) on the glass slide at 2000 rpm for 60s, which was followed by a hotplate baking step at 120°C for 120s. The two spin coated layers were then cured in an oven at 300°C for 2h. Then, 100nm layer of Si_3N_4 was deposited at room temperature on top of PI via plasma-enhanced CVD (System 100 ICP 380) for surface passivation.

Both Si/SiO_2 and PI receiver substrates underwent the same contact printing process, using the custom-built semi-automated printing system, described elsewhere [33]. Briefly, the donor and receiver substrates are mounted on a top and a bottom motorised stage, respectively. The top stage is brought in contact with the bottom one and, after this, the latter slides along one direction at a set constant velocity, for a given displacement, and maintains a selected contact pressure. For this work, the contact pressure, sliding velocity and displacement were 10 kPa, 0.1 mm/s and 6.0 mm, respectively. After contact printing, the sample of ZnO NW layer on Si/SiO_2 substrate was taken for SEM analysis, to collect data of the as-contact printed NW layer, before patterning.

C. Development of PDMS stamps for Selective removal of NWs

The trench patterned PDMS stamps were fabricated by curing a layer of PDMS on top of Si substrates patterned with negative photoresist relief structures. The Si (100)-based master template was prepared by solvent cleaning (with acetone, IPA, and DI water) and dehydration baking (2min at 115°C on a hotplate). Then, the negative epoxy-based photoresist SU-8 3025 (Microchem) was spin coated on the Si substrate in a two-step spinning: (1) 10s at 500 rpm (acceleration of 100 rpm/s), (2) 40s at 3000rpm (with an acceleration of 300 rpm/s). Following a post-spinning soft bake (15min at 95°C on a hotplate), the photoresist layers were exposed to define periodic patterns of 100 µm × 100 µm squares. After a post-exposure bake, the photoresist layers were developed with ethyl lactate (immersed for 7min 15s and manually agitated). Following rinsing and drying steps, the developed SU-8 3025 patterns were hard baked in a convection oven at 200°C for 60 min to further crosslink the epoxy-based photoresist for higher mechanical rigidity. The obtained master templates were analysed by contact profilometry (Dektak XT Contact Profiler).

To obtain the patterned elastomeric stamp, first, the PDMS based elastomer and curing agent of the Sylgard 184 Silicone Elastomer Kit by DOW were mixed in 10:1 weight ratio, respectively, and degassed for 60-90 min. In parallel, the master template surface was treated with chlorotrimethylsilane (TMCS, Sigma-Aldrich): the master templates were kept in a vacuum degassing station together with TMCS poured in a beaker until complete evaporation of the TMCS. A 4mL TMCS was added for each master template of the batch to be treated. Then, the degassed base elastomer/curing agent mixture was poured on top of the TCMS treated master template. The poured mixture was degassed again and then the templates were moved onto a levelled surface and left there to cure for at least 48h at room temperature. A final curing step was performed on a

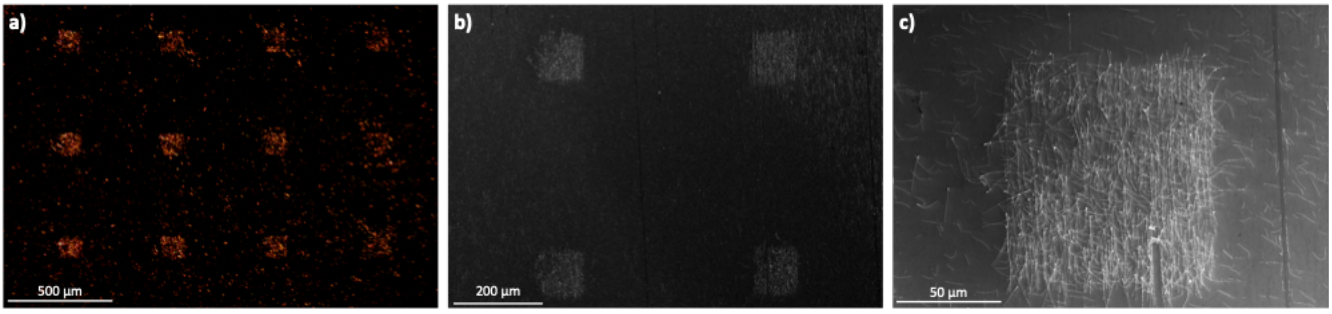

Fig. 4 a) Optical microscope and (b) SEM images of the patterned ZnO NW layer on Si/SiO_2 substrate; c) SEM image of the square-shaped NW array.

hotplate for 30min at 80°C. Finally, the PDMS stamps were obtained by peeling off the elastomer layer from the master templates. The fabricated PDMS stamps were analysed by contact profilometry, with the Dektak XT Contact Profiler.

The selective removal process was carried using the same procedure and parameters for the NW layers on both Si/SiO_2 and PI substrates. For the process, our custom-built contact printed system was used to apply a controlled pressure between the stamp and NW layer for a set time. The process was carried by exposing the patterned face of the elastomer stamp to boiling water vapours (DI water in a beaker on a hotplate at 120°C; water level to stamp distance of 7-10 cm) for 3-5s and then quickly placed on the NW layer by gently holding one edge of the stamp while progressively bringing all the stamps' surface to contact, avoiding air bobbles development. The samples with the stamp on top were mounted on the bottom stage of the contact printing system. An Ar plasma treated (60s at 100W) glass slide was mounted on the top stage, to apply uniform pressure and pick the PDMS stamp at the end of the process. The system applied a pressure of 20.5 ± 0.1 kPa for 60s. Finally, the PDMS stamp was collected and cleaned using a Scotch Magic Tape to remove the picked NWs and reused for a new run. The patterned NW array samples on Si/SiO_2 substrates were analysed via SEM.

D. All-printed photodetector fabrication and characterisation

The all-printed PDs were obtained by printing the contact electrodes on pre-patterned 3×4 ZnO NWs array on PI, using a high-resolution (line width ~1-10µm) extrusion-based DIW printer (XTPL Delta printing system). The highly viscous silver nano-paste, CL85 (over 100,000cP viscosity, 82 wt.% metal content) was used in this study as the metal electrode material. Nozzles with a 5µm opening size were used for printing and they were positioned 1µm above the substrates to avoid direct contact with NWs. The main printing parameters i.e., pressure and printing velocity, were set at 7 bars and 0.05mm/s, respectively. The printing pattern was designed to form two rectangular 200 µm × 150 µm metal contacts for each device with a 13 µm sensing channel for the UV detection. After printing, the sample was annealed at 250º C for 15 minutes to improve the electrode conductivity.

The static opto-electronic characterisations of the fabricated PDs were performed using a semiautomated 12k Autoprober and the Agilent B1500A semiconductor device parameter analyser. The PDs were probed under dark and UV LED of 365 nm of emission wavelength.

III. Results and Discussion

A. Contact printed NW layers

The VPT process led to the synthesis of NWs on the donor Si surface. A layer of aligned NWs was obtained on the receiver substrates using contact printing method. The printed NW density data was obtained with SEM analysis on a Si/SiO_2 sample. The SEM images were processed using GTFiber to obtain NW density and orientation distribution data [34]. The SEM images used for the data analysis represent an area of 31.8 µm × 22.1 µm of the NW printed sample. The NW length and area densities are 0.9 ± 0.083 μm^{-1} and 0.43 ± 0.021 μm^{-2}, respectively. Fig. 2a shows the NW angular distribution in polar coordinates (blue curve). The NWs are well aligned with a small deviation from the average alignment direction (black segment). A second set of SEM images from the same sample was obtained after selective removal to allow quantitative analysis of the removal process.

B. Analysis of Micropatterned stamp

Contact profilometry performed on three master moulds showed that the SU8-3025 pillars have an average height of ~23 ± 0.8 µm from the Si base. Fig. 3a shows the pillar structures, having quite sharp profiles. The TMCS of the mould, reducing the mould-PDMS adhesion [35, 36], resulted in an easy release of the stamp, without any damage to the micro-trenches. Thus, the exact negative replica of the mould (see Fig. 3b) was obtained. Further, the steps prevented the presence of leftover PDMS residues (as observed by optical microscopy inspection), allowing us to use the same mould for multiple stamp fabrication. The contact profilometry analysis showed that the stamp trench depth of 22.4 ± 1.3 µm. The stamps used for the selective NW removal process have a thickness of 1.9 ± 0.3 mm (optical image showing sample's cross section is included in the Supporting Information: Fig. S1) and are flexible enough to be conformally placed onto a planar surface without any evident air bubble formation.

C. Selective removal of NWs

One of the key points to achieve high removal yield is the use of a thin layer of water on the micropatterned stamp. The capillary forces developed at the NW-stamp interface, as a result of the presence of water, allow suitable adhesion during the stamp release step [37]. After selective removal, optical

TABLE I
SELECTIVE REMOVAL FIGURES OF MERIT

$\rho_{pristine}$ [μm^{-2}]	0.427 ± 0.021
ρ_{in} [μm^{-2}]	0.296 ± 0.026
ρ_{out} [μm^{-2}]	0.021 ± 0.017
Q_{NW} [%]	69.1 ± 7.02
C_{NW} [%]	93.0 ± 1.81

microscopy, and SEM images of the patterned NWs on Si/SiO_2 were acquired. Fig. 4 shows the patterned NW electronic layer after the selective removal approach. Noticeably, the periodic pattern of squares is replicated with a good fidelity, as the difference in NW density allows distinction of single squares (Fig. 4c) of NW arrays and their distances are maintained. The NW density data extracted from the SEM analysis of the sample before and after selective removal was used for quantitative analysis to evaluate the effectiveness of the removal process. In this work, we define *positive pattern* as the pattern formed by the areas where NWs should ideally remain, while the *negative pattern* refers to the areas with ideally no NW left. We express the percentage of NWs remaining in positive pattern areas after selective removal as:

$$Q_{NW}(\%) = \frac{\rho_{in}}{\rho_{pristine}} \times 100$$

where ρ_{in} is the NW area density in the positive areas of the pattern and $\rho_{pristine}$ is the initial NW area density of the contact printed NW layer. Also, we have defined the selective removal contrast as:

$$C_{NW}(\%) = \left(1 - \frac{\rho_{out}}{\rho_{in}}\right) \times 100$$

where ρ_{out} is the NW area density of the nearby regions surrounding the positive pattern. For these calculations, we decided to use area densities instead of length ones because of the sparsity of NWs in the negative pattern areas. The measured NW area densities and the calculated percentage of remaining NWs and removal contrast are summarised in Table I.

The obtained Q_{NW} is ~69%, which is lower than our previously reported value (≈92%) [29]. This could be due to the presence of water in the stamp's trenches that disturbs the positive NW pattern, particularly at the borders. This would also explain why after selective removal, a small portion of NWs is aligned perpendicular to the average alignment direction (Fig. 2b). However, most of the NWs remained aligned along the initial direction. The removal contrast is also slightly lower than the previously reported value (~99%) [29]. This can be ascribed to the fact that the stamp used in the present work is flat with a pattern of trenches, whereas the PDMS stamp used in the previous study contained a relief pattern of pillars which did not allow excess water to accumulate.

In some regions, an appreciable density of NWs was still present, whereas some NW squares in the pattern had less clear borders. The inspection of the stamps using the optical microscope after the selective removal showed that NWs are removed only from the stamps' contact area, while no NW was present inside the trenches. Therefore, the deviation from the ideal pattern cannot be ascribed to the contact of non-relief structures or stamp's unevenness. Instead, these local effects may be due to the presence of excess water at the interface layer– as the non-removed ones are completely misaligned– which prevents the effective capillary-aided stamp-NW contact. This hypothesis is also supported by previous selective removal experiments (carried out for optimisation), wherein we observed that too much water evaporated on the stamp (due to an excessive water vapours exposure time) led to no appreciable selective NW removal. Nevertheless, given the necessity to remove NWs from significantly larger substrate area, the presented results show that the patterned NW layer is obtained with a good contrast and a fair density of NWs in the positive areas. Whilst further improvement in removal yield and uniformity is possible, the obtained NW density in the active device channel is already higher than the previously reported NW patterning methods [24]. It may be noted that more than one selective removal runs were carried out using the same stamp. This is to prove that the process is resource efficient. After one process, the stamp was cleaned with the magic tape. After cleaning, no evidence of NW residues was observed under an optical microscope. The scotch tape used does not have a strong adhesion to the PDMS stamp, and thus does not cause any damage to stamp patterns. Therefore, this simple cleaning process allowed use the same stamp multiple times.

D. Printed ZnO NW-based array of photodetectors

The optimised selective removal approach was utilised to realise a patterned electronic layer of ZnO NWs on a flexible PI substrate. The as-prepared NW arrays were processed to construct a 3×4 PDs matrix. To define the sensing channel, Ag contacts were printed using DIW technique. High resolution printing of Ag yielded a sensing channel length of ~11 ± 0.6 μm, which is good enough to form stable metal-semiconductor-metal contacts on the printed NWs, as confirmed with microscopic inspections. Fig. 5a shows the fabricated array of printed PDs. These PDs were analysed with electrical measurements conducted in ambient conditions. Specifically, the time-resolved photocurrent response of the devices was recorded while they were subjected to repeated dark-UV illumination (emission wavelength of 365 nm) at calibrated illuminated UV light intensity. Fig. 5b shows the response for cycles of increasing light intensity, from 0.3 to 2.0 μW/cm^2, at a constant bias voltage. As expected, the photocurrent increases with both UV light intensity (higher electron-hole pair generation) and bias voltage V_d (higher driving field). Also, the repeatability was evaluated by running multiple dark-UV light cycles, at fixed light intensity (1.0 μW/cm^2) and bias voltage (V_d from 2.0 V to 5.0V). Fig. 5c shows that the device response to UV light is consistent for different cycles and shows a good performance. The physical explanation for the photoinduced conductance change in ZnO NWs has been thoroughly reported elsewhere [5]. Basically, in ambient atmosphere, oxygen molecules are adsorbed at the surface of ZnO NWs, and free electrons are trapped on the surface. This leads to the formation of a depletion region, which increases the device resistance. When photons having energy higher than the band gap of the

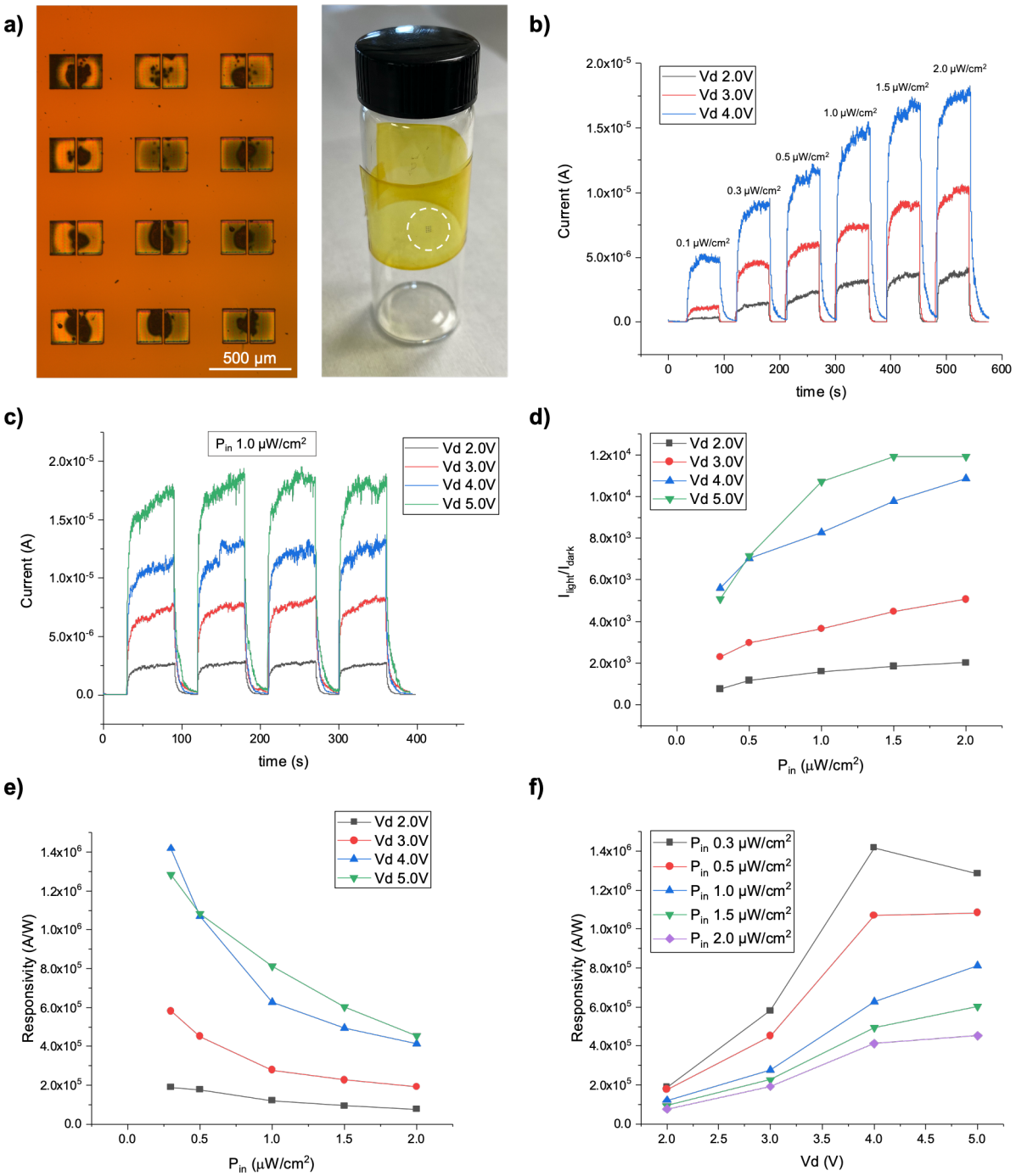

Fig. 5 a) Patterned ZnO NW layer-based photodetectors (PDs): on the left, optical microscope image of the printed PD array, on the right, overall sample of PDs on PI wrapped around a glass vial with diameter of 25 mm (devices in the circled area); b) PD dynamic photo response in ON/OFF cycles of increasing incident light intensity, at different drain voltages; c) device photo response in ON/OFF cycles at constant incident light intensity, at different drain voltages; PD's (d) light to dark current ratio and (e) responsivity trends with the incident UV light intensity, at set drain voltages; f) responsivity trend with the drain voltage, at set UV light intensities.

material are absorbed, electron-hole pairs are generated (ZnO has an energy gap of 3.34 eV, corresponding to a wavelength of 371 nm). Following this, the generated holes react with the O_2^- ions chemisorbed on the nanostructure's surface to produce molecular oxygen that is desorbed, and more free electrons are liberated from the trap sites. This contributes to increase in the conductivity of sensing channel under the illuminated conditions. The time the photocurrent takes to reach 90% of the peak light current is defined as the *response time*. When the NWs return in dark conditions, new O_2 molecules are re-absorbed, and they increase the resistivity during the *recovery time*– conventionally defined as the time taken for the current to decrease to 10% of its peak value. From the photocurrent curves recorded during dark/light cycles, the response and recovery times are found to be 28s and 13s respectively. Further extracted PD parameters used to evaluate the presented devices

performances are light to dark photocurrents ratio I_{light}/I_{dark}, the responsivity R and specific detectivity D^*. As expected, I_{light}/I_{dark} is shown to monotonically increase with increasing incident light intensity, at a constant bias voltage, with a maximum of 1.19×10^4 attained at a drain voltage V_d of 5.0 V and under UV light intensity of 2.0 μW/cm^2 (Fig. 5d). This is because a high illumination intensity is expected to generate a large number of free electrons. The sub-linear I_{light}/I_{dark} dependence on P_{in} could be explained by the saturation of trap sites by the photogenerated holes or an increase of electron trapping events with increasing free carriers density, so that fewer free electrons are liberated for each photon absorption event [38].

The responsivity is defined as [39]:

$$R=\frac{I_{light}-I_{dark}}{P_{in}\times S}$$

where P_{in} is the incident light intensity and S represents the effective sensing area of the PD. The effective sensing area is calculated by considering the NWs as cylindrical structures having an average diameter of 74 nm (as results from the fibre analysis on the SiO_2 substrate, discussed in above section III.C), covering an area of 100 μm × 11 μm (i.e., the NW square pattern length times the channel gap width) with a density of 0.296 μm^{-2} (assuming identical density to the SiO_2 substrate sample). Assuming that all the NWs in the considered area are connected to both the source and drain electrodes, the effective sensing area is 2.76×10^{-5} cm^2. Fig. 5e shows the responsivity to monotonically decrease with an increase in UV intensity due to the decrease of the I_{light}/P_{in} ratio with increasing intensities. Considering the curves at different bias voltages, it is observed that above the crossing point at 0.5 μW/cm^2, the highest I_{light}/P_{in} ratios are obtained at 4.0 V, while the absolute maximum responsivity (1.3×10^6 A/W) is obtained at 0.3 μW/cm^2 and V_d 5.0V. This very high value is due to the excellent material quality, high aspect ratio and small effective sensing area. In Fig. 5f, the data points have been rearranged to directly show the responsivity dependence on the drain voltage. The figure evidences that the responsivity monotonically increases with V_d for the incident light intensity values of 1.0 μW/cm^2 and above; whereas, for the two lowest light intensities applied, the responsivity maxima are obtained at bias voltage of 4.0 V, indicating that the free carriers available for lower UV intensities cannot provide a super-linear increase of $I_{light}(P_{in})$. Another important parameter used to evaluate the performance of PDs is the specific detectivity which allows to evaluate their capability to detect small signals. It is defined as [39]:

$$D^* = \frac{R\sqrt{S}}{\sqrt{2\times e\times I_{dark}}}$$

where e is the elemental charge. Given the proportionality between the two, the specific detectivity follows the same trend as the responsivity, with the highest value of 6.95×10^{16} Jones recorded at 0.3 μW/cm^2 and V_d 5.0V (Supporting Information Fig. S2). Next, the fabricated devices were evaluated for response uniformity. All devices in the array of printed PDs were tested through a single light/dark/light cycle with V_d 3.0 under UV light intensity of 0.1 μW/cm^2. The relevant PD parameters were extracted from their response curves and

TABLE II
DEVICE PARAMETERS FOR PDS IN THE PRINTED ARRAY

	I_{light}/I_{dark}	R (A/W)	D^* (Jones)
PD #1	1.76×10^3	2.48×10^5	1.17×10^{16}
PD #2	5.26×10^2	1.71×10^5	5.30×10^{15}
PD #3	2.26×10^3	8.18×10^5	2.40×10^{16}
PD #4	1.02×10^3	1.33×10^5	6.51×10^{15}
PD #5	8.61×10^2	8.41×10^4	4.75×10^{15}
PD #6	1.96×10^3	2.48×10^5	1.23×10^{16}
PD #7	1.37×10^3	1.68×10^5	8.49×10^{15}
PD #8	3.66×10^3	2.78×10^5	1.78×10^{16}
PD #9	1.88×10^3	2.85×10^5	1.29×10^{16}
PD #10	2.04×10^3	2.88×10^5	1.36×10^{16}
PD #11	2.07×10^3	3.07×10^5	1.41×10^{16}
PD #12	4.79×10^2	3.08×10^5	6.79×10^{15}
Average	1.66×10^3	2.78×10^5	1.15×10^{16}
Standard Deviation	8.85×10^2	1.85×10^5	5.65×10^{15}
Coefficient of variation	53.4%	66.6%	49.0%

TABLE III
COMPARISON OF RECENT ZNO NW-BASED PHOTODETECTORS (N/A, data not available; NP, nanoparticle)

Photoactive material	I_{light}/I_{dark} (peak)	Responsivity [A/W]	Specific detectivity [Jones]	Response time [s]	Recovery time [s]	Ref
ZnO NWs	10^3	3.03×10^7	$\approx10^{17}$	N/A	N/A	[40]
ZnO nanotetrapods	2.96×10^3	N/A	N/A	1.07	5.34	[41]
ZnSnO3/ZnO NWs	N/A	1.70	10^{12}	N/A	N/A	[42]
Cu2O/ZnO/ZnO NW array	N/A	3.5×10^3	5.25×10^{19}	N/A	N/A	[43]
ZNO array with CsPbBr3 QDs	2.44×10^3	0.32	1.75×10^{13}	N/A	N/A	[44]
Ga doped ZnO NW array	7.48×10^3	78.2	5.5×10^{12}	9.8	45.8	[45]
MoS2 on single ZnO	30	273	9.0×10^9	2.4×10^{-2}	N/A	[46]
Ag NPs-ZnO NWs	85.4	104	N/A	4.3	3.2	[47]
ZnO NWs	13.4	$\approx10^5$	$8.14.\times10^8$	N/A	N/A	[48]
ZnO NWs	$>10^5$	54	N/A	0.2	0.1	[5]
ZnO NWs	$>10^5$	7.50×10^6	3.3×10^{17}	0.56	0.32	[49]
ZnO NRs	$>10^3$	10^{-4}	N/A	49	25	[50]
ZnO NWs	$>10^4$	4.5×10^4	N/A	N/A	1	[51]
ZnO NWs	$>10^5$	2.6×10^3	N/A	N/A	0.28	[52]
ZnO NWs	$>10^7$	1.2×10^6	$>10^{18}$	1	N/A	[53]
ZnO NWs	$\approx10^4$	4.0	3.2×10^{14}	1.8	1.7	[54]
ZnO NWs/TPU composite	$>10^2$	30	N/A	0.8	1.6	[55]
ZnO NW patterned array	8.85×10^2	1.85×10^5	5.65×10^{15}	28	13	this work

summarised in Table II.

The considered parameters are of the same order in magnitude for all the devices. The variations could be attributed to both the NW density observed in the positive NW pattern and to the drag force of the ink while the electrodes were printed. The latter may have misaligned the NWs, which eventually hindered the formation of direct electrode/NW/electrode contacts. Further, it is well-known that it is challenging to achieve NW-metal interface uniformity among devices. Table III compares the performance of our PDs with the other state-of-the-art PDs based on ZnO NW. Despite the simplicity of the structure (not being heterostructures, decorated or doped) they have a high I_{light}/I_{dark} ratio and very high responsivity and specific detectivity. This confirms the efficacy of the selective removal approach to pattern high-grade electronic layers.

To show the flexibility and conformability of the fabricated devices, the PI substrate with devices was peeled from the glass carrier slide and wrapped around a glass vial (Fig. 5a) and conformed to convex and concave shaped printed objects (Supporting Information Fig. S3).

IV. Conclusion

In summary, we have presented a new method called 'selective removal' to develop patterned electronic layers based on inorganic NWs. The proposed method proved effective in patterning arrays of NWs with good fidelity, removal contrast and after-removal density. The optimised method was utilised to print patterned arrays of ZnO NWs on a flexible substrate which were further processed to develop all-printed PDs. The detailed opto-electrical characterisation of the fabricated arrays of PDs showed good responsivity (1.3×10^6 A/W) and specific detectivity (6.95×10^{16} Jones) in the UV range. Furthermore, high performance uniformity of the sensor array confirmed the high-grade quality of the patterned electronic layer. The presented work opens interesting avenues for lithography free high performance flexible and printed electronics. The minimum feature size that could be patterned with NWs using our approach is limited only by the photolithography resolution which is ~5µm. On the other hand, the approach can be implemented over a limitless sample area size. This is by using the same stamp multiple times on the printed nanowire layer, providing a route for large-area nanowire layer patterning.

References

[1] A. Zumeit, W. T. Navaraj, D. Shakthivel, and R. Dahiya, "Nanoribbon-based flexible high-performance transistors fabricated at room temperature," *Adv. Electron. Mater.,* vol. 6, no. 4, pp. 1901023, 2020.

[2] F. Liu, S. Deswal, A. Christou, M. Shojaei Baghini, R. Chirila, D. Shakthivel, M. Chakraborty, and R. Dahiya, "Printed synaptic transistor-based electronic skin for robots to feel and learn," *Science Robotics,* vol. 7, no. 67, pp. eabl7286, 2022.

[3] A. Kirakosyan, M. R. Sihn, M.-G. Jeon, R. M. D. Kabir, and J. Choi, "Self-aligned CH3NH3PbBr3 perovskite nanowires via dielectrophoresis for gas sensing applications," *Appl. Mater. Today,* vol. 26, pp. 101307, 2022.

[4] J. Neto, R. Chirila, A. S. Dahiya, A. Christou, D. Shakthivel, and R. Dahiya, "Skin-Inspired Thermoreceptors-Based Electronic Skin for Biomimicking Thermal Pain Reflexes," *Advanced Science*, pp. 2201525, 2022.

[5] Y. Kumaresan, G. Min, A. S. Dahiya, A. Ejaz, D. Shakthivel, and R. Dahiya, "Kirigami and Mogul-Patterned Ultra-Stretchable High-Performance ZnO Nanowires-Based Photodetector," *Adv. Mater. Technol.,* vol. 7, no. 1, pp. 2100804, 2022.

[6] D. Shakthivel, A. S. Dahiya, R. Mukherjee, and R. Dahiya, "Inorganic semiconducting nanowires for green energy solutions," *Curr. Opin. Chem. Eng.,* vol. 34, pp. 100753, 2021.

[7] G. Khandelwal, and R. Dahiya, "Self-Powered Active Sensing Based on Triboelectric Generators," *Advanced Materials,* vol. 34, no. 33, pp. 2200724, 2022.

[8] A. S. Dahiya, F. Morini, S. Boubenia, K. Nadaud, D. Alquier, and G. Poulin-Vittrant, "Organic/inorganic hybrid stretchable piezoelectric nanogenerators for self-powered wearable electronics," *Adv. Mater. Technol.,* vol. 3, no. 2, pp. 1700249, 2018.

[9] Z. Fan, J. C. Ho, Z. A. Jacobson, H. Razavi, and A. Javey, "Large-scale, heterogeneous integration of nanowire arrays for image sensor circuitry," *PNAS,* vol. 105, no. 32, pp. 11066-11070, 2008.

[10] A. Javey, Nam, R. S. Friedman, H. Yan, and C. M. Lieber, "Layer-by-Layer Assembly of Nanowires for Three-Dimensional, Multifunctional Electronics," *Nano Lett.,* vol. 7, no. 3, pp. 773-777, 2007.

[11] K. Takei, T. Takahashi, J. C. Ho, H. Ko, A. G. Gillies, P. W. Leu, R. S. Fearing, and A. Javey, "Nanowire active-matrix circuitry for low-voltage macroscale artificial skin," *Nat. Mater.,* vol. 9, no. 10, pp. 821-826, 2010.

[12] A. Zumeit, A. S. Dahiya, A. Christou, D. Shakthivel, and R. Dahiya, "Direct roll transfer printed silicon nanoribbon arrays based high-performance flexible electronics," *npj Flexible Electron.,* vol. 5, no. 1, pp. 18, 2021.

[13] R. Dahiya, D. Akinwande, and J. S. Chang, "Flexible Electronic Skin: From Humanoids to Humans [Scanning the Issue]," *Proceedings of the IEEE,* vol. 107, no. 10, pp. 2011-2015, 2019.

[14] F. Liu, S. Deswal, A. Christou, Y. Sandamirskaya, M. Kaboli, and R. Dahiya, "Neuro-inspired electronic skin for robots," *Science Robotics,* vol. 7, no. 67, pp. eabl7344, 2022.

[15] A. Zumeit, A. S. Dahiya, A. Christou, and R. Dahiya, "High performance p-channel transistors on flexible substrate using direct roll transfer stamping," *Jpn. J. Appl. Phys.,* vol. 61, no. SC1042, 2021.

[16] J. He, R. G. Nuzzo, and J. A. Rogers, "Inorganic Materials and Assembly Techniques for Flexible and Stretchable Electronics," *Proceedings of the IEEE,* vol. 103, no. 4, pp. 619-632, 2015.

[17] A. S. Dahiya, D. Shakthivel, Y. Kumaresan, A. Zumeit, A. Christou, and R. Dahiya, "High-performance printed electronics based on inorganic semiconducting nano to chip scale structures," *Nano Convergence,* vol. 7, no. 1, pp. 33, 2020.

[18] S. Acharya, A. B. Panda, N. Belman, S. Efrima, and Y. Golan, "A semiconductor-nanowire assembly of ultrahigh junction density by the Langmuir–Blodgett technique," *Adv. Mater.,* vol. 18, no. 2, pp. 210-213, 2006.

[19] O. Assad, A. M. Leshansky, B. Wang, T. Stelzner, S. Christiansen, and H. Haick, "Spray-Coating Route for Highly Aligned and Large-Scale Arrays of Nanowires," *ACS Nano,* vol. 6, no. 6, pp. 4702-4712, 2012.

[20] D. Jung, C. Lim, H. J. Shim, Y. Kim, C. Park, J. Jung, S. I. Han, S.-H. Sunwoo, K. W. Cho, and G. D. Cha, "Highly conductive and elastic nanomembrane for skin electronics," *Science,* vol. 373, no. 6558, pp. 1022-1026, 2021.

[21] R. Dahiya, "E-skin: from humanoids to humans [point of view]," *Proceedings of the IEEE,* vol. 107, no. 2, pp. 247-252, 2019.

[22] F. Liu, A. S. Dahiya, and R. Dahiya, "A flexible chip with embedded intelligence," *Nature Electronics,* vol. 3, no. 7, pp. 358-359, 2020.

[23] C. García Núñez, F. Liu, W. T. Navaraj, A. Christou, D. Shakthivel, and R. Dahiya, "Heterogeneous integration of contact-printed semiconductor nanowires for high-performance devices on large areas," *Microsyst. Nanoeng.,* vol. 4, no. 1, pp. 22, 2018.

[24] A. S. Dahiya, A. Christou, J. Neto, A. Zumeit, D. Shakthivel, and R. Dahiya, "In Tandem Contact-Transfer Printing for High-Performance Transient Electronics," *Advanced Electronic Materials,* vol. 8, no. 9, pp. 2200170, 2022.

[25] J. Yao, H. Yan, and C. M. Lieber, "A nanoscale combing technique for the large-scale assembly of highly aligned nanowires," *Nat. Nanotechnol.,* vol. 8, no. 5, pp. 329-335, 2013.

[26] D. Roßkopf, and S. Strehle, "Surface-controlled contact printing for nanowire device fabrication on a large scale," *Nanotechnology,* vol. 27, no. 18, pp. 185301, 2016.

[27] Z. Fan, J. C. Ho, Z. A. Jacobson, R. Yerushalmi, R. L. Alley, H. Razavi, and A. Javey, "Wafer-Scale Assembly of Highly Ordered Semiconductor Nanowire Arrays by Contact Printing," *Nano Lett.,* vol. 8, no. 1, pp. 20-25, 2008.

[28] M. Chakraborty, J. Kettle, and R. Dahiya, "Electronic Waste Reduction through Devices and Printed Circuit Boards designed for Circularity," *IEEE J. Flexible Electronics,* Vol. 1(1), pp 4-23, 2022.

[29] L. D. Pamphilis, A. Christou, A. S. Dahiya, and R. Dahiya, "Selective removal of contact printed nanowires for lithography-free patterning." in IEEE Int. Conf. on Flexible and Printable Sensors and Systems (FLEPS), 2022, pp. 1-4 (DOI: 10.1109/FLEPS53764.2022.9781514).

[30] D. Shakthivel, M. Ahmad, M. R. Alenezi, R. Dahiya, and S. R. P. Silva, "1D Semiconducting Nanostructures for Flexible and Large-Area Electronics: Growth Mechanisms and Suitability," Elements in Flexible and Large-Area Electronics, Cambridge University Press, 2019.

[31] D. Shakthivel, W. Navaraj, S. Champet, D. H. Gregory, and R. S. Dahiya, "Propagation of amorphous oxide nanowires via the VLS mechanism: Growth kinetics," *Nanoscale Adv.,* vol. 1, no. 9, pp. 3568-3578, 2019.

[32] C. G. Núñez, A. Vilouras, W. T. Navaraj, F. Liu, and R. Dahiya, "ZnO Nanowires-Based Flexible UV Photodetector System for Wearable Dosimetry," *IEEE Sens. J.,* vol. 18, no. 19, pp. 7881-7888, 2018.

[33] A. Christou, F. Liu, and R. Dahiya, "Development of a highly controlled system for large-area, directional printing of quasi-1D nanomaterials," *Microsyst. Nanoeng.,* vol. 7, no. 1, pp. 82, 2021.

[34] N. E. Persson, J. Rafshoon, K. Naghshpour, T. Fast, P.-H. Chu, M. McBride, B. Risteen, M. Grover, and E. Reichmanis, "High-Throughput Image Analysis of Fibrillar Materials: A Case Study on Polymer Nanofiber Packing, Alignment, and Defects in Organic Field Effect Transistors," *ACS Appl. Mater. Interfaces,* vol. 9, no. 41, pp. 36090-36102, 2017.

[35] J. Cheon, and S. Kim, "Fabrication and Demonstration of a 3D-printing/PDMS Integrated Microfluidic Device," *Recent Progress in Materials,* vol. 4, no. 1, pp. 1-1, 2022.

[36] R. Guo, L. Qi, L. Xu, B. Li, and H. Zou, "A novel hybrid patterning technique for polymer PDMS micro and nanoscale nozzle by double casting," *J. Manuf. Processes,* vol. 75, pp. 711-718, 2022.

[37] X. Ma, Q. Liu, D. Xu, Y. Zhu, S. Kim, Y. Cui, L. Zhong, and M. Liu, "Capillary-Force-Assisted Clean-Stamp Transfer of Two-Dimensional Materials," *Nano Letters,* vol. 17, no. 11, pp. 6961-6967, 2017.

[38] B. Mallampati, S. V. Nair, H. E. Ruda, and U. Philipose, "ZnO Nanowire Based Photoconductor with High Photoconductive Gain," *MRS Online Proceedings Library,* vol. 1805, no. 1, pp. 932, 2015.

[39] Z. Liu, T. Luo, B. Liang, G. Chen, G. Yu, X. Xie, D. Chen, and G. Shen, "High-detectivity InAs nanowire photodetectors with spectral response from ultraviolet to near-infrared," *Nano Research,* vol. 6, no. 11, pp. 775-783, 2013.

[40] S. Ma, A. S. Dahiya, A. Christou, and R. Dahiya, "All-printed ZnO nanowire based high performance photodetectors." in IEEE Int. Conf. on Flexible and Printable Sensors and Systems (FLEPS), 2022, pp. 1-4, DOI: 10.1109/FLEPS53764.2022.9781570..

[41] M. Ilickas, R. Mardosaitė, B. Abakevičienė, and S. Račkauskas, "Room temperature ZnO nanowire UV sensors by spray-coating." in IEEE Int. Conf. on Flexible and Printable Sensors and Systems (FLEPS), 2022 pp. 1-4, doi: 10.1109/FLEPS53764.2022.9781537.

[42] C. Tuc Altaf, O. Coskun, A. Kumtepe, M. Sankir, and N. Demirci Sankir, "Bifunctional ZnO nanowire/ZnSnO3 heterojunction thin films for photoelectrochemical water splitting and photodetector applications," *Materials Letters,* vol. 322, pp. 132450, 2022.

[43] X. Fei, D. Jiang, and M. Zhao, "Gaining Effect of Flower-Like Zno Nanowire Arrays on the Responsivity Performance of Cu2o/Zno Heterojunction Detector," *Available at SSRN 4093979*.

[44] J.-F. Tang, Y.-D. Sie, Z.-L. Tseng, J.-H. Lin, L.-C. Chen, and C.-L. Hsu, "Perovskite Quantum Dot–ZnO Nanowire Composites for Ultraviolet–Visible Photodetectors," *ACS Applied Nano Materials,* vol. 5, no. 5, pp. 7237-7245, 2022.

[45] N. Xu, Z. Yuan, B. Wang, F. Nie, J. He, and X. Wang, "Significant improvement in the performance of well-aligned ZnO nanowire arrays ultraviolet photodetector by Ga doping," *Microelectronic Engineering,* vol. 260, pp. 111787, 2022.

[46] X.-L. Zhang, J. Li, B. Leng, L. Yang, Y.-D. Song, S.-Y. Feng, L.-Z. Feng, Z.-T. Liu, Z.-W. Fu, X. Jiang, and B.-D. Liu, "High-performance ultraviolet-visible photodetector with high sensitivity and fast response speed based on MoS2-on-ZnO photogating heterojunction," *Tungsten*, 2022.

[47] Y. Noh, J. Shin, H. Lee, G. Y. Kim, M. Kumar, and D. Lee, "Decoration of Ag Nanoparticle on ZnO Nanowire by Intense Pulsed Light and Enhanced UV Photodetector," *Chemosensors,* vol. 9, no. 11, pp. 321, 2021.

[48] C.-H. Lin, D.-S. Tsai, T.-C. Wei, D.-H. Lien, J.-J. Ke, C.-H. Su, J.-Y. Sun, Y.-C. Liao, and J.-H. He, "Highly deformable origami paper photodetector arrays," *ACS nano,* vol. 11, no. 10, pp. 10230-10235, 2017.

[49] X. Liu, L. Gu, Q. Zhang, J. Wu, Y. Long, and Z. Fan, "All-printable band-edge modulated ZnO nanowire photodetectors with ultra-high detectivity," *Nature communications,* vol. 5, no. 1, pp. 1-9, 2014.

[50] J. Kim, H. Park, and S.-H. Jeong, "A kirigami concept for transparent and stretchable nanofiber networks-based conductors and UV photodetectors," *Journal of Industrial and Engineering Chemistry,* vol. 82, pp. 144-152, 2020.

[51] Q. Yang, X. Guo, W. Wang, Y. Zhang, S. Xu, D. H. Lien, and Z. L. Wang, "Enhancing Sensitivity of a Single ZnO Micro-/Nanowire Photodetector by Piezo-phototronic Effect," *ACS Nano,* vol. 4, no. 10, pp. 6285-6291, 2010.

[52] G. Cheng, X. Wu, B. Liu, B. Li, X. Zhang, and Z. Du, "ZnO nanowire Schottky barrier ultraviolet photodetector with high sensitivity and fast recovery speed," *Applied Physics Letters,* vol. 99, no. 20, pp. 203105, 2011.

[53] T. Chen, X. Gao, J.-Y. Zhang, J.-L. Xu, and S.-D. Wang, "Ultrasensitive ZnO Nanowire Photodetectors with a Polymer Electret Interlayer for Minimizing Dark Current," *Advanced Optical Materials,* vol. 8, no. 4, pp. 1901289, 2020.

[54] Y. Li, Y. Li, J. Chen, Z. Sun, Z. Li, X. Han, P. Li, X. Lin, R. Liu, and Y. Ma, "Full-solution processed all-nanowire flexible and transparent ultraviolet photodetectors," *Journal of Materials Chemistry C,* vol. 6, no. 43, pp. 11666-11672, 2018.
[55] D.-H. Lien, H.-P. Wang, S.-B. Chen, Y.-C. Chi, C.-L. Wu, G.-R. Lin, Y.-C. Liao, and J.-H. He, "360° omnidirectional, printable and transparent photodetectors for flexible optoelectronics," *npj Flexible Electronics,* vol. 2, no. 1, pp. 19, 2018.

Luca De Pamphilis received his Bachelor's and Master's (Hons.) degrees in Materials Engineering and Nanotechnology in Polytechnic University of Milan, Italy, in 2013 and 2017, respectively. He is currently pursuing his Ph.D. in the Bendable Electronics and Sensing Technologies group in the James Watt School of Engineering, University of Glasgow. UK. His research interests encompass large-area compatible nanofabrication and memristive devices.

Abhishek S. Dahiya is Research Associate in Bendable Electronics and Sensing Technologies (BEST) group at the University of Glasgow. He received Ph.D. from the GREMAN laboratory, Université François Rabelais de Tours, France in 2016. He has done postdoctoral work at various CNRS laboratories in France: GREMAN (2016-2017), ICMCB (2018-2019), and IES/LIRMM (2019-2020). His research interest includes synthesis of nanomaterials, nanofabrication, energy harvesting, and printed and flexible electronics.

Adamos Christou is a PhD student at the University of Glasgow, U.K., studying Electrical and Electronic Engineering at the James Watt School of Engineering as a member of the Bendable Electronics and Sensing Technologies (BEST) Group. He received a B.Eng. (Hons.) degree in Mechatronics Engineering from the University of Glasgow in 2018.

Sihang Ma received her B.Eng. (Hons.) degree in Electrical and Electronics Engineering from the University of Glasgow, U.K., in 2020. She is currently pursing Ph.D. at Bendable Electronics and Sensing Technologies (BEST) group in the James Watt School of Engineering, University of Glasgow, U.K. Her research interest includes the development of ultra-thin chips and ultra-thin chip based printed flexible electronics.

Ravinder Dahiya (Fellow, IEEE) is Professor in ECE Department at Northeastern University, Boston, USA. He is the leader of Bendable Electronics and Sustainable Technologies (BEST) research group (formerly, Bendable Electronics and Sensing Technologies (BEST) group). His group conducts fundamental and applied research in flexible and printable electronics, tactile sensing, electronic skin, robotics, and wearable systems. He has authored or co-authored about 500 publications, books and submitted/granted patents and disclosures. He has led several international projects. He is President (2022-23) of the IEEE Sensors Council. He is the Founding Editor in Chief of IEEE JOURNAL ON FLEXIBLE ELECTRONICS (J-FLEX) and has served on the editorial boards of IEEE SENSORS JOURNAL (2012-2020) and IEEE TRANSACTIONS ON ROBOTICS (2012-2017). He was the Technical Program co-chair of IEEE Sensors 2017 and IEEE Sensors 2018 and has been General Chair/Co-Chair of several conferences including IEEE FLEPS (2019, 2020, 2021), which he founded in 2019, and IEEE Sensors 2023. He is recipient of EPSRC Fellowship, Marie Curie and Japanese Monbusho Fellowships. He has received several awards, including 2016 Microelectronic Engineering Young Investigator Award (Elsevier), 2016 Technical Achievement Award from the IEEE Sensors Council and 12 best paper awards as author/co-author in International Conferences and Journal.